

# Ising superconductivity in monolayer niobium dichalcogenide alloys

Darshana Wickramaratne

Center for Computational Materials Science, U.S. Naval Research Laboratory, Washington, DC 20375, USA

I.I. Mazin

Department of Physics and Astronomy, George Mason University, Fairfax, VA 22030, USA and  
Quantum Science and Engineering Center, George Mason University, Fairfax, VA 22030, USA

(Dated: August 16, 2021)

NbSe<sub>2</sub> and NbS<sub>2</sub> are isostructural two-dimensional materials that exhibit contrasting superconducting properties when reduced to the single monolayer limit. Monolayer NbSe<sub>2</sub> is an Ising superconductor, while there have been no reports of superconductivity in monolayer NbS<sub>2</sub>. NbS<sub>x</sub>Se<sub>2-x</sub> alloys exhibit an intriguing non-monotonic dependence of the superconducting transition temperature with sulfur content, which has been interpreted as a manifestation of fractal superconductivity. However, several key questions about this result are not known: (1) Does the electronic structure of the alloy differ from the parent compounds, (2) Are spin fluctuations which have been shown to be prominent in monolayer NbSe<sub>2</sub> also present in the alloys? Using first-principles calculations, we show that the density of states at the Fermi level and the proximity to magnetism in NbS<sub>x</sub>Se<sub>2-x</sub> alloys are both reduced compared to the parent compound; the former would decrease the transition temperature while the latter would increase it. We also show that Se vacancies, which are likely magnetic pair-breaking defects, may form in large concentrations in NbSe<sub>2</sub>. Based on our results, we suggest an alternative explanation of the non-monotonic behavior the superconducting transition temperature in NbS<sub>x</sub>Se<sub>2-x</sub> alloys, which does not require the conjecture of multifractality.

## I. INTRODUCTION

Ising superconductivity in two-dimensional materials is a rapidly growing field of theoretical and experimental research [1–8]. The combination of broken-inversion symmetry and strong spin-orbit coupling present in single monolayers (MLs) of the two-dimensional transition metal dichalcogenides leads to Fermi surfaces where the pseudospin of the electrons is perpendicular to the plane of the monolayer and the pseudospin direction flips between time-reversal invariant points of the Brillouin zone. This has been experimentally confirmed by establishing, for example in NbSe<sub>2</sub>, that the superconducting critical field is significantly higher in-plane versus out-of-plane, and much larger than the Pauli limit [1]. While there have been extensive phenomenological descriptions of Ising superconductivity, there are several intriguing material-specific puzzles.

In NbSe<sub>2</sub>, which is the most widely studied Ising superconductor, the superconducting transition temperature,  $T_c$ , decreases from  $\sim 6$  K to  $\sim 3 - 4$  K, when it is reduced from bulk to a single monolayer [1]. Similar studies conducted on NbS<sub>2</sub> provide an intriguing contrast. In 2H-NbS<sub>2</sub>  $T_c$  is  $\sim 6$  K, while superconductivity has not been observed in bulk 3R-NbS<sub>2</sub> [9, 10]. These two polytypes differ in the stacking of the individual monolayers, while within each ML Nb atoms are in a trigonal prismatic coordination with the chalcogen atom, similar to NbSe<sub>2</sub>. Reducing the thickness of NbS<sub>2</sub> leads to a strong suppression in  $T_c$  [11]. Superconductivity has not been found in ML NbS<sub>2</sub>.

It was recently reported that when ML NbSe<sub>2</sub> is alloyed with sulfur, the  $T_c$  increases up to the sulfur content of  $x=0.2$  [12] in ML NbS<sub>x</sub>Se<sub>2-x</sub> alloys. For sulfur content

greater than  $\sim 0.3$ , the  $T_c$  was then found to decrease monotonically [12] exhibiting qualitatively similar behavior to the bulk alloys. This non-monotonic change in  $T_c$  of the ML alloys, which is in contrast to the monotonic reduction in  $T_c$  in bulk NbS<sub>x</sub>Se<sub>2-x</sub> alloys [13, 14], was interpreted as disorder-induced enhancement of  $T_c$  which possibly arises from the multifractality of the electronic wave functions [15, 16]. Implicit in this assumption is that the role of alloying on electronic and Coulomb interactions is sufficiently weak so as to not impact  $T_c$  directly. While this is an enticing consideration, there are several important questions and experimental puzzles that need to be addressed first, which we briefly outline.

The measurements where fractal superconductivity was observed report a  $T_c$  for ML NbSe<sub>2</sub> that is  $\sim 2$  K lower than the widely accepted  $T_c$  of ML NbSe<sub>2</sub>,  $\sim 3$  to 4 K [1, 5]. In fact, the peak  $T_c$  where fractal superconductivity is observed is  $\sim 3$  K, which occurs for  $0.2 \leq x \leq 0.5$ . We also note the experimental in-plane lattice constant is relatively unchanged for  $0 \leq x \leq 0.2$  [17]. If the  $T_c$  of NbSe<sub>2</sub> in Ref. [12] occurred at the more widely accepted 3 to 4 K, this would not lead to a dome-shaped dependence of  $T_c$  on sulfur content, as illustrated in Fig.1. Instead,  $T_c$  would decrease linearly with sulfur content, as has been found when sulfur is alloyed into bulk NbSe<sub>2</sub> [13, 14].

Taken together, we arrive at three possible mechanisms that can lead to this non-monotonic dependence of  $T_c$  on sulfur content. The first is the role of fractal superconductivity, which was invoked in Refs. [12, 18]. While this exotic phenomenon may lead to a non-monotonic change in  $T_c$  [19], the success of this model requires information on a plethora of material-dependent parameters that are often not accessible by experiment alone. A second pos-

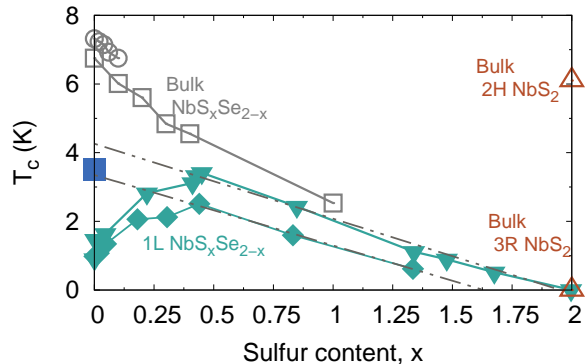


FIG. 1. Experimental reports of the superconducting transition temperature versus alloy concentration in bulk and ML  $\text{NbS}_x\text{Se}_{2-x}$  alloys as a function of sulfur content,  $x$ . The references associated with each marker is as follows:  $\square$  [14],  $\circ$  [13],  $\nabla$  and  $\diamond$ , [12],  $\triangle$  [10] and  $\blacksquare$  [1]. Open symbols correspond to measurements on bulk samples while filled symbols correspond to measurements on ML samples. The dotted lines correspond to a linear extrapolation of the ML data for  $x > 0.3$ . See the main text for the discussion on the extrapolation.

sible mechanism is the role of the charge-density wave (CDW), which has been shown to lead to a pseudogapping of the Fermi surface in ML  $\text{NbSe}_2$  [20, 21], and thus to a reduction in  $T_c$ . However, recent studies have suggested the CDW transition temperature varies little when  $\text{NbSe}_2$  transitions from bulk to a single ML [22, 23], while  $T_c$  exhibits a large change [1]. This would imply that the coupling between the superconducting and CDW order parameters is weak, as has been found in studies on bulk  $\text{NbSe}_2$  [24, 25].

A third mechanism is the collective role of point defects [4] and spin fluctuations [6], both of which have been suggested as a source of pair breaking in ML  $\text{NbSe}_2$ . Experimental studies on ML  $\text{NbSe}_2$  have found the selenium vacancy concentration can be large (equivalent to a bulk concentration of  $\sim 10^{21} \text{ cm}^{-3}$ ), depending on the growth conditions [26]. Selenium vacancies, which are likely magnetic point defects in  $\text{NbSe}_2$  [27], can act as a source of pair-breaking and decrease  $T_c$ . However, during the growth of  $\text{NbS}_x\text{Se}_{2-x}$  alloys in the presence of sulfur, which is isovalent to selenium, but more electronegative, it can occupy the selenium vacancies and lower the concentration of pair-breaking defects. This is analogous to the finding that oxygen can substitute for sulfur (both of which are isovalent) in sulfur-deficient ML  $\text{TaS}_2$ , and lead to an increase in  $T_c$  compared to ML  $\text{TaS}_2$ . [28].

Alloying will also lead to changes in the electronic structure, which may also affect the proximity of the material to magnetism or lead to changes in the density of states (DOS) at the Fermi level, and therefore  $T_c$ . There is *a priori* no means to determine how all of these properties change with alloying. Furthermore, if defects are

indeed the source of the lower  $T_c$  in  $\text{NbSe}_2$ , this raises questions on the purported relationship between the non-monotonic dependence of  $T_c$  on sulfur content, and fractal superconductivity [12].

In the present work we propose an alternative solution that reconciles these puzzles. Using first-principles density functional theory calculations (Sec. V) we show that this non-monotonic dependence of  $T_c$  on sulfur content can emerge from the interplay between defects and the effect of alloying on the electronic structure and spin-fluctuations. We show that sulfur is completely miscible in  $\text{NbSe}_2$ , across the entire alloy composition range. For finite concentrations of sulfur in  $\text{NbS}_x\text{Se}_{2-x}$  we find a reduction of the density of states at the Fermi level *and* a weakening of magnetism, compared to the parent compounds,  $\text{NbSe}_2$  and  $\text{NbS}_2$ . We conjecture a combination of these effects can lead to a non-monotonic dependence of  $T_c$  on sulfur content, without having to invoke the phenomenon of multifractality.

## II. RESULTS

We start by considering the properties of chalcogen vacancies in  $\text{NbS}_2$  and  $\text{NbSe}_2$  in the dilute limit. The formation energies of a sulfur vacancy,  $V_S$ , in  $\text{NbS}_2$  and a selenium vacancy,  $V_{Se}$ , in  $\text{NbSe}_2$  is listed in Table I. The

TABLE I. Formation energy of chalcogen vacancies in  $\text{NbSe}_2$  and  $\text{NbS}_2$  under Nb-rich and Nb-poor conditions.

Defect	Nb-rich (eV)	Nb-poor (eV)
$V_{Se}$	0.7	1.7
$V_S$	1.2	2

results show that the formation energy of  $V_{Se}$  is lower than  $V_S$ , even under Se-rich conditions that were used in the growth of the  $\text{NbSe}_2$  samples in Ref. [12]. This suggests that as-grown ML  $\text{NbSe}_2$  is likely to have a higher concentration of selenium vacancies compared to sulfur vacancies in  $\text{NbS}_2$ . We also considered the possibility that sulfur may substitute on the Nb site and calculated the formation energy of this defect,  $S_{Nb}$ , in ML  $\text{NbSe}_2$ . In the dilute limit we find the formation energy of  $S_{Nb}$  to be larger than the formation energy of  $V_{Se}$ . Hence, for the purposes of alloying beyond the dilute limit we only consider substitution of S on the Se site.

Next we check the stability of  $\text{NbS}_x\text{Se}_{2-x}$  alloys with respect to decomposing into their parent compounds,  $\text{NbSe}_2$  and  $\text{NbS}_2$ . Figure 2 illustrates the lowest enthalpy structure for each composition. We find the  $T = 0 \text{ K}$  formation enthalpy across the entire range of compositions is negative which suggests ordered  $\text{NbS}_x\text{Se}_{2-x}$  alloys are stable with respect to decomposition into the parent compounds.

We now turn to the electronic and magnetic properties of the alloys. We first consider the parent compounds,

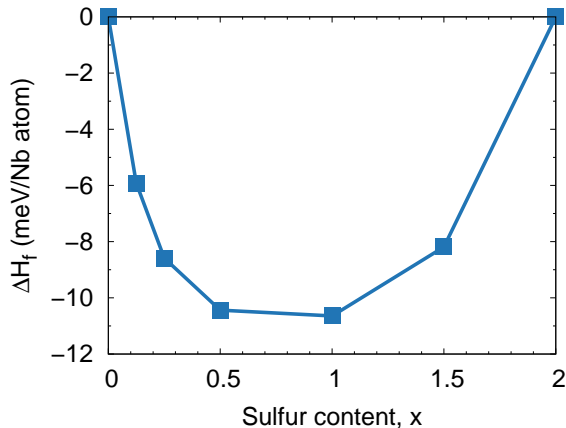


FIG. 2. Formation enthalpy as a function of sulfur content,  $x$ , in  $\text{NbS}_x\text{Se}_{2-x}$

$\text{NbSe}_2$  and  $\text{NbS}_2$ . In a single ML the Nb atoms are in a trigonal prismatic coordination with the chalcogen atoms. In ML  $\text{NbSe}_2$  the trigonal crystal field that acts on the  $4d$  states of  $\text{Nb}^{4+}$  leads to one band that crosses the Fermi level, which generates Fermi contours at  $\Gamma$ , K and  $K'$  [6]. The combination of broken inversion symmetry in the monolayer and strong spin-orbit coupling leads to a spin-orbit splitting of the spin degenerate band along the M-K- $\Gamma$  line of the Brillouin zone. Since the  $4d$  states of  $\text{Nb}^{4+}$  in  $\text{NbS}_2$  are also in a trigonal prismatic coordination, albeit with a shorter Nb-S bond length compared to the Nb-Se bond length, the qualitative features of the band structure between the two materials are similar [17].

ML  $\text{NbSe}_2$  exhibits strong spin fluctuations, which have been highlighted as a potential source of pair breaking [6, 29–31]. First-principles calculations have shown that monolayer  $\text{NbSe}_2$  can host ferromagnetic spin fluctuations with a sizeable Stoner renormalization, and an antiferromagnetic spin spiral state with  $\mathbf{q}$  vector  $(0.2, 0, 0)$  [6, 30]. In ML  $\text{NbSe}_2$  we find the spin spiral state to be 1.7 meV/Nb atom lower in energy compared to the non-magnetic state. In  $\text{NbS}_2$ , we find a spin spiral state at a  $\mathbf{q}$ -vector of  $(0.2, 0, 0)$  is also stable [17] and is 1.9 meV/Nb atom lower in energy compared to the non-magnetic ground state. If spin fluctuations are sizeable in the alloy they can impact pairing interactions.

To study the effect of alloying on the spin spiral energies we use virtual crystal approximation (VCA) calculations (Sec. V) for sulfur contents that correspond to  $x=0.5, 1$  and  $1.5$ . Figure 3(a) illustrates the energy difference between the spin spiral state with respect to the non-magnetic state,  $\Delta E_{\text{spiral}}$ , in  $\text{NbS}_x\text{Se}_{2-x}$ . When sulfur is alloyed into  $\text{NbSe}_2$ , the spin spiral state is less stable for intermediate values of sulfur content than for either  $\text{NbSe}_2$  and  $\text{NbS}_2$ . At  $x=1$  we find  $\Delta E_{\text{spiral}}$  decreases by a factor of 2.1 compared to  $\text{NbS}_2$  where the magnitude of  $\Delta E_{\text{spiral}}$  is the largest. The magnitude of the magnetic moment on the Nb atom is also suppressed by up to  $\simeq 25\%$  in the spin-spiral state for the alloys with fi-

nite sulfur content compared to the parent compounds, as illustrated in Fig. 3(a).

Next we consider whether ferromagnetic spin fluctuations, which are present in  $\text{NbSe}_2$ , are also impacted due to alloying by using the VCA and collinear fixed-spin moment calculations for ML  $\text{NbSe}_2$ ,  $\text{NbS}_2$ ,  $\text{NbSSe}$ ,  $\text{NbS}_{1.5}\text{Se}_{0.5}$ , and  $\text{NbS}_{0.5}\text{Se}_{1.5}$ . We fit these FSM calculations (illustrated in Fig. 3(b)) to the following expression,  $E(m) = a_0 + a_1 m^2 + a_2 m^4 + a_3 m^6 + a_4 m^8$ , where  $E(m)$  is the total energy for a given magnetization  $m$ . The quantity of interest is the ferromagnetic spin susceptibility,  $\chi$ , which is defined as  $\chi = a_2^{-1} = \left(\frac{\delta^2 E}{\delta m^2}\right)^{-1}$ . We find  $\chi$  varies non-monotonically as a function of sulfur content as illustrated in the inset of Fig. 3(b), where it is large for  $\text{NbSe}_2$  and  $\text{NbS}_2$  and suppressed in the case of the alloys. Hence, it is reasonable to assume that the spin fluctuations for intermediate concentrations are suppressed non-monotonically for all relevant wave vectors. In both cases these fluctuations are the weakest at roughly equal concentrations of S and Se.

The origin of the reduction in  $\chi$  (and, probably, also  $\Delta E_{\text{spiral}}$ , given the relatively small spiral vector of  $(0.2, 0, 0)$ ) can be understood by examining the density of states (DOS). The DOS at the Fermi level,  $N(E_F)$  as a function of sulfur content is illustrated in Fig. 3(c). In  $\text{NbSe}_2$  and  $\text{NbS}_2$ ,  $N(E_F)$  is suppressed from 2.8 states/eV/Nb atom in the nonmagnetic structure to 2.14 states/eV/Nb atom in  $\text{NbSe}_2$  and 2.18 states/eV/Nb atom in  $\text{NbS}_2$  in the spin spiral ground state [17]. We also find  $N(E_F)$  is suppressed for the alloys at  $x=0.5, 1$ , and  $1.5$ , where in the non-magnetic state  $N(E_F)$  is  $\sim 2.5$  states/eV/Nb atom while in the spin spiral state it reduces to 1.9 states/eV/Nb atom. Hence, for the parent compounds and the alloys, our calculations indicate there is a gain in one-electron energy by transitioning to the spin spiral state. We also find that in the spin spiral state, the magnitude of  $N(E_F)$  of the alloys decreases by 10% compared to  $N(E_F)$  of the parent compounds. Such a small change in  $N(E_F)$  as a function of sulfur content is consistent with the fact that  $N(E_F)$  is comprised almost entirely of Nb  $d$ -states in  $\text{NbSe}_2$  and  $\text{NbS}_2$ .

### III. DISCUSSION

Our calculations lead to two general features that will play an important role in superconductivity in  $\text{NbS}_x\text{Se}_{2-x}$  alloys. First, the formation energy of selenium vacancies in  $\text{NbSe}_2$  is low, which is consistent with large concentrations of  $V_{\text{Se}}$  found in as-grown  $\text{NbSe}_2$ . Since they are likely magnetic [27],  $V_{\text{Se}}$  can act as a source of pair-breaking, which would manifest in a reduction in  $T_c$ . This is consistent with measurements on ML  $\text{NbSe}_2$ , where low values of  $T_c$  are found in samples where the residual resistivity ratio is low [26]. Our calculations show that the substitution of sulfur on the selenium site in  $\text{NbSe}_2$  is energetically favorable for all sulfur composi-

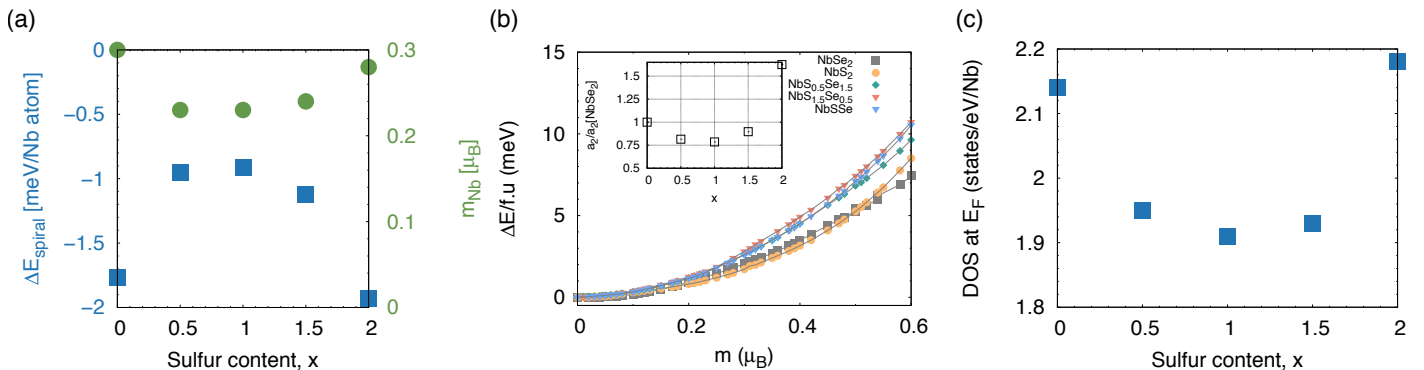


FIG. 3. (a) Energy difference between the spin spiral state and the non magnetic state as a function of sulfur content,  $x$ , in  $\text{NbS}_x\text{Se}_{2-x}$  (blue, left vertical axis – ■). Magnetic moment per Nb atom as a function of sulfur content in the spin spiral calculation with finite  $q$  (green, right vertical axis – ○). (b) Collinear fixed-spin moment calculations of  $\text{NbSe}_2$  (grey – ■),  $\text{NbS}_2$  (orange – ○),  $\text{NbS}_{0.5}\text{Se}_{1.5}$  (teal – ◇),  $\text{NbSSe}$  (red – ▽), and  $\text{NbS}_{1.5}\text{Se}_{0.5}$  (blue – △) illustrate the change in energy per formula unit with respect to the non-magnetic state as a function of magnetic moment per Nb atom. The inset illustrates the coefficient  $a_2$  (see main text) normalized by the value of  $a_2$  in  $\text{NbSe}_2$ . (c) Density of states at the Fermi level,  $E_F$ , as a function of sulfur content,  $x$ . The magnitude of the DOS for  $\text{NbSe}_2$  and  $\text{NbS}_2$  correspond to the spin spiral state [17].

tions. Hence, during the growth of  $\text{NbS}_x\text{Se}_{2-x}$  we expect sulfur to occupy the sites of missing selenium atoms up to a critical sulfur composition. This would lower the concentration of pair-breaking  $V_{\text{Se}}$  defects. This immediately explains why the putative multifractal behavior was observed in  $\text{NbSe}_2$  samples with suppressed  $T_c$ , compared to the samples in the literature with lower defect concentrations, which is correlated with higher  $T_c$ .

Second, we find that both  $\text{NbSe}_2$  and  $\text{NbS}_2$  host strong spin fluctuations at all wave vectors. However, for finite sulfur compositions in  $\text{NbS}_x\text{Se}_{2-x}$  this tendency towards magnetism is weakened, which favors superconductivity. This reduction in the proximity to magnetism competes with a reduction in  $N(E_F)$  of the alloys compared to  $\text{NbSe}_2$  and  $\text{NbS}_2$ , which would decrease the electron-phonon coupling constant,  $\lambda_{ep}$ , and weaken superconductivity. We can estimate the sign of the net effect using the general expression derived in Ref. [32], under a simplifying assumption that the spin-fluctuations and phonons have comparable frequencies. Then  $d \log T_c / d \log \lambda_{ep} \propto \lambda_{ep} + 2 \lambda_{ep} \lambda_{sf}$ , and  $-d \log T_c / d \log \lambda_{sf} \propto \lambda_{sf} + 2 \lambda_{sf} \lambda_{ep}$ . The DOS is reduced by  $\approx 10\%$  between the end composition and the midpoint. In contrast, the tendency to magnetism, as measured by the spin-spiral energy gain, decreases by a factor of 2, between the end composition and the midpoint. The latter is expected to be more important, at least for low concentrations of sulfur.

Taken together, these two features collectively imply that the non-monotonic dependence of  $T_c$  on sulfur content [12] is not sufficient proof of fractal superconductivity, but likely has a rather prosaic origin: it is sulfur occupying a high concentration of selenium vacancy sites (thus decreasing the concentration of pair-breaking defects), which is accompanied by a strong reduction of the tendency to magnetism as the sulfur concentration increases from 0 to  $\sim 0.5$ . This effect overlaps with the general weakening of the electron-phonon matrix elements,

as evidenced by the smaller coupling constant in  $\text{NbS}_2$  compared to  $\text{NbSe}_2$ , despite their similar  $N(E_F)$ . [33–35]

We can also show that of the two effects (defects versus reduction in tendency to magnetism) that lead to the increase of  $T_c$  from  $x = 0$  to  $x = 0.5$ , the former is more important. Indeed, if we linearly extrapolate the  $T_c(x)$  data for  $x \geq 0.3$  to  $x = 0$ , we get a  $T_c$  of  $\text{NbSe}_2$  that ranges from 3.35 K to 4.2 K, as illustrated in Fig. 1, which is close to the  $T_c$  reported for ML  $\text{NbSe}_2$  that has a lower concentration of defects [26].

#### IV. CONCLUSIONS

In conclusion, we have presented a detailed analysis of the properties of  $\text{NbS}_x\text{Se}_{2-x}$  alloys using first-principles calculations. Our results, when analyzed in the context of recent studies that have asserted the presence of fractal superconductivity in  $\text{NbS}_x\text{Se}_{2-x}$  alloys [12, 18], suggest multifractality isn't the only mechanism that can lead to non-monotonic changes in  $T_c$  in these alloys. The following key factors emerge from our calculations: (1) the low formation energy of selenium vacancies that are magnetic pair-breaking point defects, (2) the stability of  $\text{NbS}_x\text{Se}_{2-x}$  alloys across the entire composition range with respect to decomposition into the parent compounds, (3) the reduction in the density of states at the Fermi level as a function of alloy content in  $\text{NbS}_x\text{Se}_{2-x}$  and (4) a reduction in the proximity to magnetism in  $\text{NbS}_x\text{Se}_{2-x}$  alloys compared to  $\text{NbSe}_2$  and  $\text{NbS}_2$ .

These results suggest that as-grown  $\text{NbSe}_2$  hosts a large concentration of pair-breaking selenium vacancies that upon alloying are occupied by sulfur atoms. This leads to an increase in  $T_c$  up to a critical composition where the sulfur concentration is equal to concentration of selenium vacancies that are initially present during the growth. For larger  $x$ ,  $T_c$  monotonically decreases

reflecting general weakening of the electron-phonon matrix elements toward NbS<sub>2</sub>. These two distinct regimes manifest in a non-monotonic change in  $T_c$ . Given that disorder-induced non-monotonic changes in  $T_c$  have been observed in other transition metal dichalcogenide alloys due to isovalent substitution [36–38], we expect our findings to open new avenues for investigation in this broad class of materials.

## V. METHODS

Our calculations are based on density functional theory within the projector-augmented wave method [39] as implemented in the VASP code [40, 41] using the generalized gradient approximation defined by the Perdew-Burke-Ernzerhof (PBE) functional [42]. We found it is essential that Nb  $5s^1, 4s^2, 4p^6, 4d^4$  electrons and Se  $4s^2, 4p^4$  electrons are treated as valence. All calculations use a plane-wave energy cutoff of 400 eV. We use a  $(18 \times 18 \times 1)$   $\Gamma$ -centered  $k$ -point grid for the monolayer structure when performing structural optimization and calculating the electronic structure. The cell shape and atomic positions of each structure was optimized using a force convergence criteria of 5 meV/Å.

For the defect calculations we use a  $(10 \times 10 \times 1)$  supercell of ML NbSe<sub>2</sub> and NbS<sub>2</sub>. To simulate a chalcogen vacancy we remove a single chalcogen atom (S atom in NbS<sub>2</sub> and Se atom in NbSe<sub>2</sub>), relax all of the atomic coordinates and determine the total energy. The formation energy, of for example, a selenium vacancy,  $V_{\text{Se}}$  in NbSe<sub>2</sub> is defined as:

$$E^f(V_{\text{Se}}) = E_{\text{tot}}(V_{\text{Se}}) - E_{\text{tot}}(\text{NbSe}_2) - \mu_{\text{Se}} \quad (1)$$

where  $E^f(V_{\text{Se}})$  is the formation energy of the selenium vacancy,  $E_{\text{tot}}(V_{\text{Se}})$  is the total energy of the NbSe<sub>2</sub> defect supercell with a selenium vacancy,  $E_{\text{tot}}(\text{NbSe}_2)$  is the total energy of the pristine NbSe<sub>2</sub> supercell, and  $\mu_{\text{Se}}$  is the chemical potential of selenium. All of the defect calculations were performed with a  $(3 \times 3 \times 1)$   $k$ -point grid.

For the calculations of the alloy properties we consider two approaches; the virtual crystal approximation (VCA) and explicit supercell calculations using either a  $(4 \times 1 \times 1)$  and a  $(4 \times 4 \times 1)$  supercell that is constructed from the unit cell of the ML structure. For each alloy supercell we consider different arrangements of the S and Se atoms for compositions corresponding to  $x=0.125, 0.25, 0.5, 1$ , and 1.5, and relax all of the atomic positions. The  $k$ -point grid for structural relaxation of each supercell is scaled with respect to the  $(18 \times 18 \times 1)$   $\Gamma$ -centered  $k$ -point grid we use for calculations of the unit cell.

To determine the thermodynamics of alloy formation we calculated the formation enthalpy,  $\Delta H(x)$ , as a function of sulfur content,  $x$ , using the  $(4 \times 4 \times 1)$  supercell.  $\Delta H(x)$  is defined as:

$$\Delta H(x) = E(x) - xE(\text{NbS}_2) - (1-x)E(\text{NbSe}_2) \quad (2)$$

where  $E(x)$  is the total energy of the alloy supercell with sulfur content,  $x$ ,  $E(\text{NbS}_2)$  is the total energy of the NbS<sub>2</sub> supercell and  $E(\text{NbSe}_2)$  is the total energy of the NbSe<sub>2</sub> supercell.

We varied the lattice parameters for each alloy configuration linearly as a function of sulfur content in accordance with Vegard’s law and then relax all of the atomic coordinates. For a given sulfur content,  $x$ , the in-plane lattice constant,  $a(\text{NbS}_x\text{Se}_{2-x})$  was varied as  $a(\text{NbS}_x\text{Se}_{2-x}) = xa_{\text{NbS}_2} + (2-x)a_{\text{NbSe}_2}$ , where  $a_{\text{NbS}_2}$  is the in-plane lattice parameter of bulk NbS<sub>2</sub> and  $a_{\text{NbSe}_2}$  is the in-plane lattice parameter of bulk NbSe<sub>2</sub>. We verified the accuracy of Vegard’s law for a subset of alloy structures by allowing the lattice parameters and atomic positions to relax. In all cases, the variation of the in-plane lattice parameters was linear [17].

To calculate the spin spiral energies we used the generalized Bloch theorem formalism [43] as implemented within VASP. We use a dense  $(36 \times 36 \times 1)$   $\Gamma$ -centered  $k$ -point grid for the unit cell. We determine the energy difference between the spin spiral state with respect to the non-magnetic state,  $\Delta E_{\text{spiral}}$ , which is defined as  $\Delta E_{\text{spiral}} = E(\mathbf{q}) - E(\mathbf{q} = \mathbf{0})$  where  $E(\mathbf{q})$  is the total energy of the unit cell with spin spiral wavevector  $\mathbf{q}$  and  $E(\mathbf{q} = \mathbf{0})$  is the total energy of the non-magnetic unitcell.

To determine the ferromagnetic spin susceptibility,  $\chi$  we used collinear fixed-spin moment (FSM) calculations (sometimes referred to as the constrained local moments approach). In our collinear FSM calculations we constrain the magnitude of the magnetic moment on the Nb atom. Performing these calculations allows us to determine the change in energy with respect to the non-magnetic ground state as a function of the total magnetization,  $m$ . We then fit our results to an expansion of the total energy as a function of  $m$  (see main text to determine  $\chi$ ). The spin susceptibility,  $\chi$ , obtained from FSM calculations is sensitive to the choice in energy convergence threshold, and the number of magnetization values used in the fit to expansion in the total energy as a function of magnetic moment. We use an energy convergence threshold of  $10^{-8}$  eV, and up to 50 magnetization versus energy points between  $0 \mu_B$  and  $0.6 \mu_B$  for all of the FSM calculations.

The results on the formation enthalpy of the alloys are obtained using a  $(4 \times 4 \times 1)$  supercell with tetrahedron smearing and a  $(9 \times 9 \times 1)$   $k$ -point grid. The spin spiral energies, fixed spin moment calculations, and the density of states of the alloys are obtained using VCA calculations for sulfur contents that correspond to  $x=0.5, 1$ , and 1.5. The VCA calculations use the same  $k$ -point grid as the unit cell calculations. The in-plane lattice parameters for the  $x=0.5, 1$ , and 1.5 VCA calculations are scaled linearly according to Vegard’s law. Furthermore, we also interpolate the vertical Nb-chalcogen bond length along the  $c$ -axis for each VCA alloy calculation.

## ACKNOWLEDGEMENTS

We thank Mikhail Feigel'man and Roxana Margine for helpful discussions. D.W. was supported by the Office of

Naval Research (ONR) through the Naval Research Laboratory's Basic Research Program. I.I.M. was supported by ONR through grant N00014-20-1-2345. Calculations by D.W. were performed at the DoD Major Shared Resource Center at AFRL.

- 
- [1] X. Xi, Z. Wang, W. Zhao, J.-H. Park, K. T. Law, H. Berger, L. Forró, J. Shan, and K. F. Mak, *Nat. Phys.* **12**, 139 (2016).
- [2] J. Lu, O. Zheliuk, I. Leermakers, N. F. Yuan, U. Zeitler, K. T. Law, and J. Ye, *Science* **350**, 1353 (2015).
- [3] B. T. Zhou, N. F. Yuan, H.-L. Jiang, and K. T. Law, *Phys. Rev. B* **93**, 180501 (2016).
- [4] D. Möckli and M. Khodas, *Phys. Rev. B* **101**, 014510 (2020).
- [5] C. Sergio, M. R. Sinko, D. P. Gopalan, N. Sivadas, K. L. Seyler, K. Watanabe, T. Taniguchi, A. W. Tsun, X. Xu, D. Xiao, and B. Hunt, *Nat. Comm.* **9**, 1427 (2018).
- [6] D. Wickramaratne, S. Khmelevskiy, D. F. Agterberg, and I. Mazin, *Phys. Rev. X* **10**, 041003 (2020).
- [7] D. Costanzo, H. Zhang, B. A. Reddy, H. Berger, and A. F. Morpurgo, *Nat. Nano* **13**, 483 (2018).
- [8] Y. Saito, Y. Nakamura, M. S. Bahramy, Y. Kohama, J. Ye, Y. Kasahara, Y. Nakagawa, M. Onga, M. Tokunaga, T. Nojima, *et al.*, *Nat. Phys.* **12**, 144 (2016).
- [9] I. Guillamón, H. Suderow, S. Vieira, L. Cario, P. Diener, and P. Rodiere, *Phys. Rev. Lett.* **101**, 166407 (2008).
- [10] C. Witteveen, K. Górnicka, J. Chang, M. Månsson, T. Klimczuk, and F. O. von Rohr, *Dalton Transactions* **50**, 3216 (2021).
- [11] R. Yan, G. Khalsa, B. T. Schaefer, A. Jarjour, S. Rouvimov, K. C. Nowack, H. G. Xing, and D. Jena, *Applied Physics Express* **12**, 023008 (2019).
- [12] K. Zhao, H. Lin, X. Xiao, W. Huang, W. Yao, M. Yan, Y. Xing, Q. Zhang, Z.-X. Li, S. Hoshino, *et al.*, *Nat. Phys.* **15**, 904 (2019).
- [13] H. Luo, J. Strychalska-Nowak, J. Li, J. Tao, T. Klimczuk, and R. J. Cava, *Chemistry of Materials* **29**, 3704 (2017).
- [14] K. Sugawara, K. Yokota, J. Takemoto, Y. Tanokura, and T. Sekine, *Journal of low temperature physics* **91**, 39 (1993).
- [15] M. Feigel'man, L. Ioffe, V. Kravtsov, and E. Cuevas, *Annals of Physics* **325**, 1390 (2010).
- [16] I. Burmistrov, I. Gornyi, and A. Mirlin, *Phys. Rev. Lett.* **111**, 066601 (2013).
- [17] See Supplemental Material at [url] for additional details.
- [18] C. Rubio-Verdu, A. M. Garcia-Garcia, H. Ryu, D.-J. Choi, J. Zaldivar, S. Tang, B. Fan, Z.-X. Shen, S.-K. Mo, J. I. Pascual, and M. M. Ugeda, *Nano Letters* **20**, 5111 (2020), PMID: 32463696, <https://doi.org/10.1021/acs.nanolett.0c01288>.
- [19] B. Sacépé, M. Feigel'man, and T. M. Klapwijk, *Nature Physics* **16**, 734 (2020).
- [20] M. Calandra, I. Mazin, and F. Mauri, *Phys. Rev. B* **80**, 241108 (2009).
- [21] C.-S. Lian, C. Si, and W. Duan, *Nano Lett.* **18**, 2924 (2018).
- [22] M. M. Ugeda, A. J. Bradley, Y. Zhang, S. Onishi, Y. Chen, W. Ruan, C. Ojeda-Aristizabal, H. Ryu, M. T. Edmonds, H.-Z. Tsai, A. Riss, S.-K. Mo, D. Lee, A. Zettl, Z. Hussain, Z.-X. Shen, and M. Crommie, *Nat. Phys.* **12**, 92 (2016).
- [23] R. Bianco, L. Monacelli, M. Calandra, F. Mauri, and I. Errea, *Phys. Rev. Lett.* **125**, 106101 (2020).
- [24] M. Leroux, I. Errea, M. Le Tacon, S.-M. Souliou, G. Garbarino, L. Cario, A. Bosak, F. Mauri, M. Calandra, and P. Rodière, *Phys. Rev. B* **92**, 140303 (2015).
- [25] K. Cho, M. Kończykowski, S. Teknowijoyo, M. A. Tanatar, J. Guss, P. Gartin, J. M. Wilde, A. Kreyssig, R. McQueeney, A. I. Goldman, *et al.*, *Nat. Comm.* **9**, 1 (2018).
- [26] H. Wang, X. Huang, J. Lin, J. Cui, Y. Chen, C. Zhu, F. Liu, Q. Zeng, J. Zhou, P. Yu, *et al.*, *Nat. Comm.* **8**, 1 (2017).
- [27] D. Wickramaratne, M. Haim, M. Khodas, and I. I. Mazin, *Phys. Rev. B* **104**, L060501 (2021).
- [28] J. Bekaert, E. Khestanova, D. G. Hopkinson, J. Birkbeck, N. Clark, M. Zhu, D. A. Bandurin, R. Gorbachev, S. Fairclough, Y. Zou, *et al.*, *Nano letters* **20**, 3808 (2020).
- [29] S. Divilov, W. Wan, P. Dreher, E. Bölen, D. Sánchez-Portal, M. M. Ugeda, and F. Ynduráin, *Journal of Physics: Condensed Matter* **33**, 295804 (2021).
- [30] S. Das and I. I. Mazin, arXiv preprint arXiv:2104.13205 (2021).
- [31] W. Wan, P. Dreher, R. Harsh, F. Guinea, and M. M. Ugeda, arXiv preprint arXiv:2101.04050 (2021).
- [32] O. V. Dolgov, I. I. Mazin, A. A. Golubov, S. Y. Savrasov, and E. G. Maksimov, *Phys. Rev. Lett.* **95**, 257003 (2005).
- [33] C. Heil, S. Poncé, H. Lambert, M. Schlipf, E. R. Margine, and F. Giustino, *Phys. Rev. Lett.* **119**, 087003 (2017).
- [34] E. Margine and *et. al.*, "In preparation".
- [35] A. Anikin, R. D. Schaller, G. P. Wiederrecht, E. R. Margine, I. I. Mazin, and G. Karapetrov, *Phys. Rev. B* **102**, 205139 (2020).
- [36] J. Peng, Z. Yu, J. Wu, Y. Zhou, Y. Guo, Z. Li, J. Zhao, C. Wu, and Y. Xie, *ACS nano* **12**, 9461 (2018).
- [37] L. Li, X. Deng, Z. Wang, Y. Liu, M. Abeykoon, E. Dooryhee, A. Tomic, Y. Huang, J. B. Warren, E. S. Bozin, *et al.*, *npj Quantum Materials* **2**, 1 (2017).
- [38] H. Luo, W. Xie, J. Tao, H. Inoue, A. Gyenis, J. W. Krizan, A. Yazdani, Y. Zhu, and R. J. Cava, *Proceedings of the National Academy of Sciences* **112**, E1174 (2015).
- [39] P. E. Blöchl, *Phys. Rev. B* **50**, 17953 (1994).
- [40] G. Kresse and J. Hafner, *Phys. Rev. B* **47**, 558 (1993).
- [41] G. Kresse and J. Furthmüller, *Phys. Rev. B* **54**, 11169 (1996).
- [42] J. P. Perdew, K. Burke, and M. Ernzerhof, *Phys. Rev. Lett.* **77**, 3865 (1996).
- [43] L. Sandratskii, *Journal of Physics: Condensed Matter* **3**, 8565 (1991).